Acta Crystallographica Section B
Structural Science
ISSN 0108-7681

Structural study of $K_xNa_{1-x}NbO_3$ (KNN) for compositions in the range x = 0.24–0.36

D. W. Baker,[a]* P. A. Thomas,[a] N. Zhang[b] and A. M. Glazer[b]

[a]Department of Physics, University of Warwick, England, and [b]Department of Physics, University of Oxford, England

Correspondence e-mail: d.w.baker@warwick.ac.uk

Received 8 August 2008
Accepted 11 November 2008

The structure of the *A*-site substituted perovskite $K_xNa_{1-x}NbO_3$, x = 0.24–0.36, where a phase boundary was previously reported, has been determined by high-resolution X-ray powder and neutron powder diffraction studies. The structure of the x = 0.3 compound was refined in the monoclinic space group *Pm* at 293 K and in *P*4*mm* at 523 K. The Glazer tilt system of the room-temperature monoclinic phase is $a^0b^+c^0$, which has implications for the nature of the next symmetry change with composition towards pure potassium niobate. A phase-coexistence region at the transition between monoclinic and tetragonal phases was also identified, consistent with a first-order phase boundary. There is also evidence for an intermediate oxygen-octahedra tilted tetragonal phase.

1. Introduction

In recent years there has been much interest in finding a suitable replacement for the archetypal piezoelectric material lead zirconium titanate, $Pb(Zr_{1-x}Ti_x)O_3$ (PZT), because it contains lead. One of the front runners in lead-free piezoelectrics is potassium sodium niobate ($K_xNa_{1-x}NbO_3$, denoted here by KNNx%). The phase diagram for KNNx was originally reported by Ahtee & Glazer (1976) and shows a phase boundary at $x = 0.5$. Considerable attention has been focused on this composition, which has been referred to as exhibiting a morphotropic phase boundary (MPB) by a number of workers (*e.g.* Birol *et al.*, 2006; Zhang *et al.*, 2008; Shrout & Zhang, 2007; Guo *et al.*, 2004). The term MPB was first coined by Jaffe *et al.* (1955) to describe the particular phase boundary in PZT that occurs at about 48% molar substitution of Ti for Zr, where the symmetry changes abruptly from rhombohedral (R) to tetragonal (T) over a negligibly small compositional range and where the boundary remains approximately constant with temperature, *i.e.* there is a quasi-vertical line in the phase diagram. The concept of a *morphotropic* phase boundary should not, therefore, be confused with the type of phase boundary normally encountered in phase diagrams, which is not usually temperature-independent. Importantly, physical properties such as the dielectric permittivity, the electromechanical coupling factor, the piezoelectric coefficients and the remanent polarization are enhanced in the vicinity of the MPB. Therefore, it is natural in searching for a lead-free analogue of PZT to investigate systems, such as KNN, in which there are phase boundaries that may show MPB-like behaviour. It is not in the remit of this paper to attempt a review of the vast literature concerning the MPB in PZT; however, it should be noted that even in PZT, there is considerable controversy about the true nature of the MPB. Noheda *et al.*

Table 1
Refinement details for KNN30 at 293 and 523 K.

	293 K	523 K
Crystal data		
Chemical formula	$K_{0.3}Na_{0.7}NbO_3$	$K_{0.3}Na_{0.7}NbO_3$
M_r	168.73	168.73
Cell setting, space group	Monoclinic, *Pm*	Tetragonal, *P4mm*
Tilt system	$a^0b^+c^0$	$a^0a^0a^0$
Temperature (K)	293	523
a, *b*, *c* (Å)	5.64304 (5), 3.93187 (2), 5.61260 (5)	3.95092 (1), 3.95092 (1), 4.00852 (2)
β (°)	89.914 (1)	90
V (Å^3)	124.53 (1)	62.57 (1)
Z	2	1
D_x (g cm^{-3})	4.500	4.478
Radiation type	Neutron TOF	Neutron TOF
Specimen form, colour	Powder, white	Powder, white
Specimen preparation cooling rate (K min^{-1})	3	3
Specimen preparation pressure (kPa)	100	100
Specimen preparation temperature (K)	1373	1373
Data collection		
Diffractometer	HRPD	HRPD
Data collection method	Specimen mounting: vanadium can packed with powder; mode: reflection; scan method: time-of-flight	Specimen mounting: vanadium can packed with powder; mode: reflection; scan method: time-of-flight
Refinement		
Refinement on	F^2	F^2
R factors	R_p = 0.091, R_{wp} = 0.081, R_{exp} = 0.125, R_{Bragg} = 0.027, S = 0.65	R_p = 0.063, R_{wp} = 0.067, R_{exp} = 0.128, R_{Bragg} = 0.021, S = 0.53
Excluded region(s)	None	None
Profile function	TOF pseudo-Voigt	TOF pseudo-Voigt
No. refined parameters	42	24
Weighting scheme	1 if $Y_{obs} \leq 1$, $1/\sigma Y_{obs}$ otherwise	1 if $Y_{obs} \leq 1$, $1/\sigma Y_{obs}$ otherwise
$(\Delta/\sigma)_{max}$	< 0.0001	< 0.0001
d_{min}, d_{max}	~ 0.6 to 4.6	~ 0.6 to 4.6

(2000) showed the existence of an intermediate phase of monoclinic (M) symmetry sandwiched between the R and T phases at the MPB, which simultaneously explained why R and T phases do not have to coexist at this boundary and provided an explanation for the enhanced piezoelectric effects *via* the mechanism of polarization rotation. Glazer *et al.* (2004) argued that the local symmetry of PZT in the R phase is actually monoclinic and described the transition from R to T through the M phase *via* growth and dimunition of short-range order, whereas Ragini, Mishra & Pandey (2002) dispensed with R symmetry altogether, instead refining the structure as monoclinic variants of the perovskite structure on the Zr-rich side of the boundary. Meanwhile, Rossetti *et al.* (2008) view the behaviour of PZT in terms of a system of adaptive ferroelectric nanodomain states.

According to Ahtee & Glazer (1976), the boundary at $x = 0.5$ is from orthorhombic symmetry (*Amm*2) on the K-rich side to monoclinic symmetry (*Pm*) on the Na-rich side. These space groups are subgroup-related and we have found that the phase change appears to be continuous, within the limits of the discrete compositional changes achievable during the synthesis of ceramics (Baker & Thomas, 2009). Most current research on this system is focused on lowering the high-temperature ferroelastic phase transition from orthorhombic to tetragonal at 473 K towards room temperature by the addition of various extra dopants. This phase change is now frequently termed the polymorphic phase transition (PPT; Shrout & Zhang, 2007; Zhang *et al.*, 2007; Du *et al.*, 2008), which refers to the fact that the unit cell changes shape.

KNN50 has a piezoelectric constant d_{33} value of 127 pCN^{-1} (Jaeger & Egerton, 1962), which is of the same order of magnitude as un-doped PZT, which has a d_{33} value originally reported to be 200 pCN^{-1} (Jaffe *et al.*, 1971). Both materials can be doped to increase this value, as is well summarized in Saito *et al.* (2004). It is clear that KNN is potentially a good candidate to replace PZT, and also has the advantage of having three reported phase boundaries that may be MPBs in the phase diagram (Ahtee & Glazer, 1976). However, little or no work has been carried out on the two boundaries at $x = 0.3$ and $x = 0.17$. In this paper, a comprehensive study of the $x = 0.3$ region of the phase diagram is reported. A change to the originally suggested oxygen-octahedral tilt system for KNN30 is found in both the room-temperature and high-temperature phases, which could lead to considerable interest in terms of the physical properties in this composition range. Also reported for the first time is a phase coexistence region at the monoclinic to tetragonal phase transition at 523 K, firmly establishing its first-order nature.

2. Experimental

2.1. Sample preparation

Polycrystalline samples of KNN were prepared by the conventional solid-state reaction method. The starting materials were reagent-grade powders of Nb_2O_5 (99.9985%), K_2CO_3 (99.995%) and Na_2CO_3 (99.995%) in the correct stoichiometric ratios, stored in air-tight containers. The powders were ball-milled in ethanol with alumina balls for 72 h, before being pressed into pellets. These were embedded in a powder bed of the same compostion in order to reduce the loss of potassium and sodium through volatilization, and placed in a closed platinum crucible. The pellets were calcined at 1073 K for 10 h, then ground, re-pelleted and sintered (again in a powder bed) at 1373 K for 4 h. All heating and cooling rates were 180 K h^{-1}. Sample compositions were

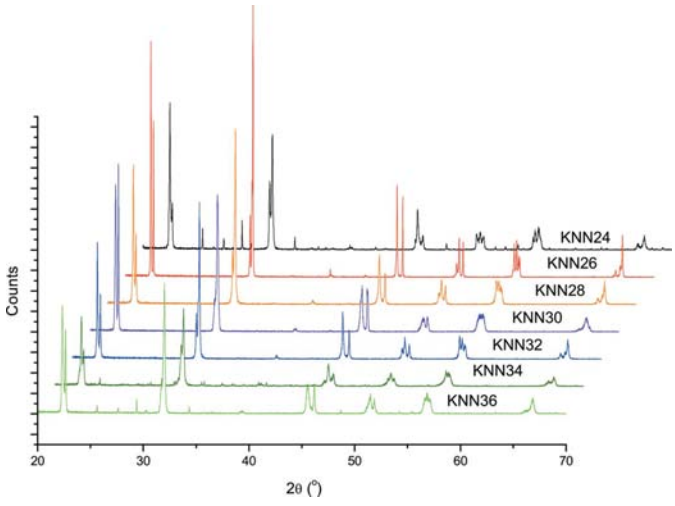

Figure 1
Powder X-ray diffraction scans of KNN24 to KNN36 using a Panalytical MPD with Cu $K\alpha_1$ radiation in Bragg–Brentano geometry.

checked using variable-pressure energy-dispersive X-ray analysis (EDX) on a Zeiss Supra 55VP FEG SEM with EDAX *Genesis* software.

2.2. Time-of-flight (TOF) neutron study

Scans of KNN30 were recorded on the high-resolution powder diffractometer at ISIS, UK. Scans (2 h) were taken at room temperature and at two points in the tetragonal phase region (523 and 623 K), as well as 10 min scans every 10 K in the temperature range from 293 to 723 K. Details of the experiment and refinement of the room-temperature monoclinic phase and the high-temperature tetragonal phase are presented in Tables 1 and 2.[1]

2.3. X-ray powder diffraction

θ–2θ scans (Fig. 1) of KNN from $x = 0.24$ to 0.36 were also performed on a Panalytical X'Pert Pro multipurpose X-ray diffraction system (MPD) with a curved Johansson monochromator, providing focused Cu $K\alpha_1$ radiation. The setup included an X'Celerator detector with a high count rate and an excellent signal-to-noise ratio, so that the oxygen-octahedra tilt peaks would be clearly visible. Even after sintering there was some variation in the quality of the samples produced, despite the fact that all were created under the same conditions. This variation indicates that the procedure is sensitive to any moisture present during the creation process, as both the raw materials and the final product are known to be slightly hygroscopic.

High-temperature measurements were performed with an Anton Paar HTK 1200 N furnace. Scans around the monoclinic to tetragonal phase transition of KNN26 at 473–483 K are shown in Fig. 2. The tilt peaks of the monoclinic phase (at around 35.7 and 42.7°2θ) exhibit interesting behaviour in this temperature range, whereby they reduce in intensity and split further apart. Detailed analysis of the phase transition at 473 K showed the existence of a phase coexistence region over a 10 K range, as seen in Fig. 3. The model was refined as a combination of the monoclinic *Pm* and tetragonal *P*4*mm* structures. The extra peaks that do not index on either structure are thought to be that of a parasitic perovskite phase. They appear as leading edges to the main monoclinic peaks, both at room temperature (Fig. 1) and at the high-temperature phase transition (Fig. 3). Their appearance on the low-angle side of the KNN26 peaks suggest that they belong to a relatively potassium-rich perovskite phase.

Table 2
Octahedral angles (°) for *Pm* at 293 K.

O6—Nb1—O6	163.1 (1)	O5—Nb2—O5	168.1 (2)
O1—Nb1—O3	171.2 (1)	O1—Nb2—O3	174.0 (2)
O2—Nb1—O4	166.0 (1)	O2—Nb2—O4	167.6 (2)

3. Discussion

3.1. Rietveld refinement of KNN30

The diffraction data for KNN30 obtained from HRPD were initially treated by the Pawley refinement method to obtain suggestions for the crystal system and the unit cell. This automatic procedure returned monoclinic and orthorhombic solutions with high figures of merit. Examination of the diffraction patterns revealed a number of reflections that are observed as a consequence of lowering the symmetry due to

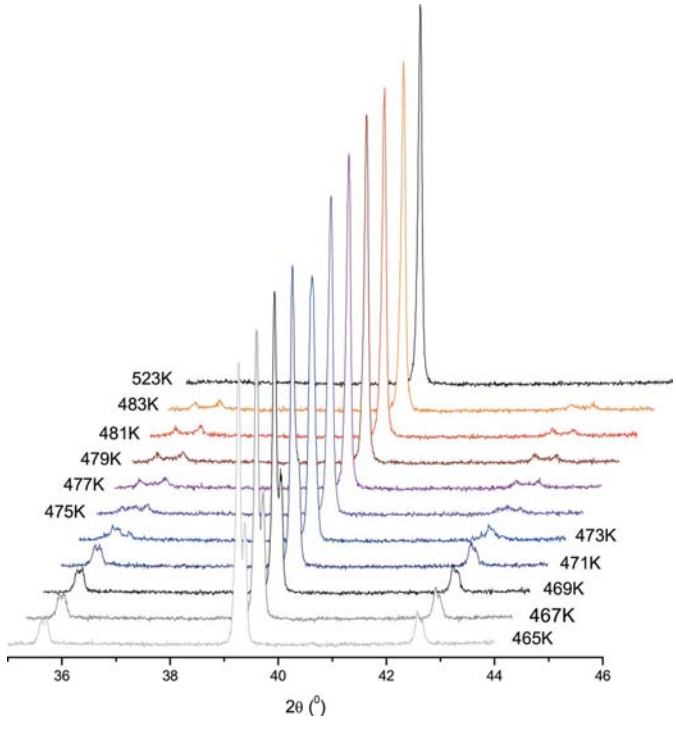

Figure 2
High-temperature scans showing the oxygen-octahedra tilt peaks in the coexistence region for KNN26, obtained by X-ray powder diffraction.

[1] Supplementary data for this paper are available from the IUCr electronic archives (Reference: KD5027). Services for accessing these data are described at the back of the journal.

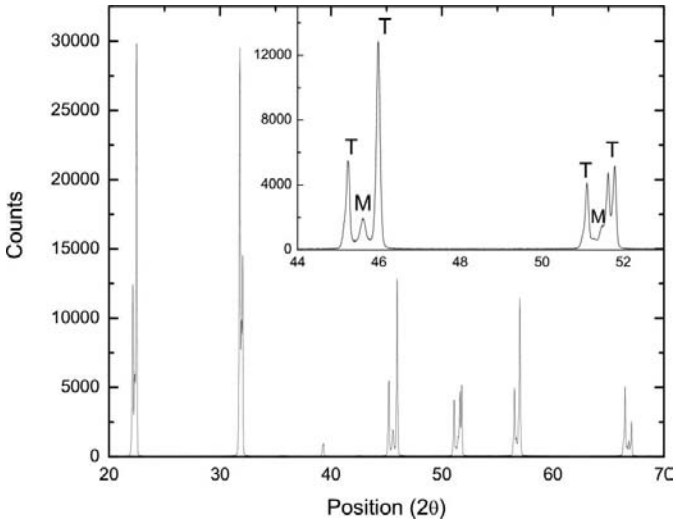

Figure 3
X-ray powder diffraction scan showing the coexistence of phases of KNN26 at the monoclinic tetragonal boundary. Peaks labelled M are the monoclinic phase, with T representing the tetragonal phase.

the displacement of the O atoms associated with the tilting of the octahedra (referred to elsewhere as oxygen tilt peaks). These tilt peaks, when indexed on a doubled perovskite cell of side ~ 8 Å, were found to be of the type 301, 321 *etc*. (Fig. 4), which are indicative of the presence of a b^+ tilt in the Glazer notation (Glazer, 1975). It is important to note that there are no peaks characteristic of minus tilts in the patterns for any of the samples having compositions $x = 0.24$ to 0.36. This is in contradiction to Glazer and Ahtee's phase diagram where these compositions are assigned to 'phase K' and the tilt system $a^-b^+c^0$ (Fig. 5). There is also another superstructure peak with indices 323 on the doubled cell, which must arise from cation ordering as it cannot be an oxygen tilt peak. Refinements by the Rietveld profile-fitting method were performed with *TOPAS Academic* (Coelho, 2004) for both neutron and X-ray powder diffraction data in both orthorhombic (*Amm2*) and monoclinic symmetries (*Pm, Cm*). The best fit (Fig. 6) to the room-temperature data was achieved for a structure described by the non-centrosymmetric monoclinic space group *Pm* on the rhombic setting (Table 1) of the perovskite unit cell and supporting one in-phase b^+ tilt of the oxygen octahedra and two-dimensional cation displacements in the (010) mirror plane. Referring to the generalization by Stokes *et al.* (2002) of the Glazer notation to include cation displacements, this corresponds to the classification $a^0_+b^+_0c^0_+$, where the superscripts denote the octahedral tilts and the subscripts the cation displacements. The possibility that there could be more than one plus tilt was investigated extensively, including attempts at refinement in space group *Cm* on a different setting of the unit cell (Stokes *et al.*, 2002). This was tried because there was some ambiguity over whether there was an a^+ or c^+ tilt present in addition to the b^+ tilt. There was no significant improvement to the structural model on the assumption of two tilts and all peaks could be explained by the single tilt: thus, the simpler *Pm* model with the single plus tilt was adopted.

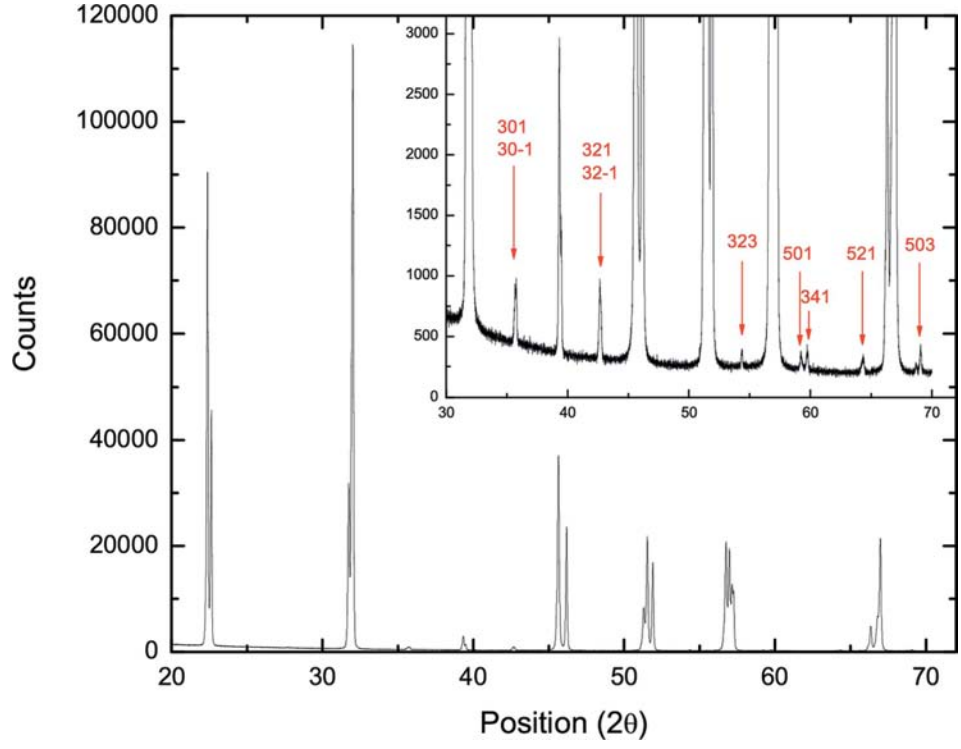

Figure 4
Tilt peaks exhibited by KNN26 on the doubled pseudo-cubic perovskite cell from a powder X-ray scan, using a Panalytical MPD.

3.2. Detector peak shape

Some effort went into characterizing the peak shape for the X'Celerator detector, as the peaks for all samples were found to be more asymmetric than expected when compared with a silicon standard sample, measured both with the X'Celerator detector and a proportional counter for comparison. In *TOPAS Academic* (Coelho, 2004), the modified Thompson–Cox–Hastings pseudo-Voigt (TCHZ) peak shape gave the best fit, but still could not fully account for the asymmetry. The approach of deriving the peak profile from the fundamental detector parameters offered little improvement. The 'Full Axial Model' gave the best fit to the peak shape (Fig. 7), but not all of the instrumental parameters refined to sensible values. Filament length, sample length and receiving slit length refined to the expected

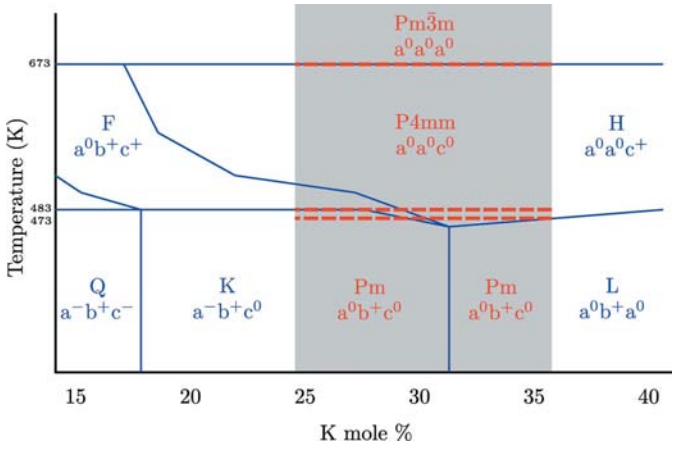

Figure 5
The revised phase diagram for KNN produced as a result of this study. The grey shaded region shows the assignments of this paper from $x = 0.24$ to $x = 0.36$ (with our proposed space groups in red), superimposed on the 1976 phase diagram of Ahtee and Glazer, denoted in blue. The region enclosed by the dotted red lines shows the width of the two-phase monoclinic–tetragonal region.

values, but the Soller slit values were at least twice as large as the expected size (0.002 rad.). It was decided that the best approach was to use the 'Simple Axial Model' function, as it only contains one refinable parameter (receiving slit length) which refined very close to the correct value (9.54 ± 0.05 mm compared with 10 mm), and gave a fit comparable to that of the 'Full Axial Model' approach. This method was adopted for all structural refinements from X-ray data reported here.

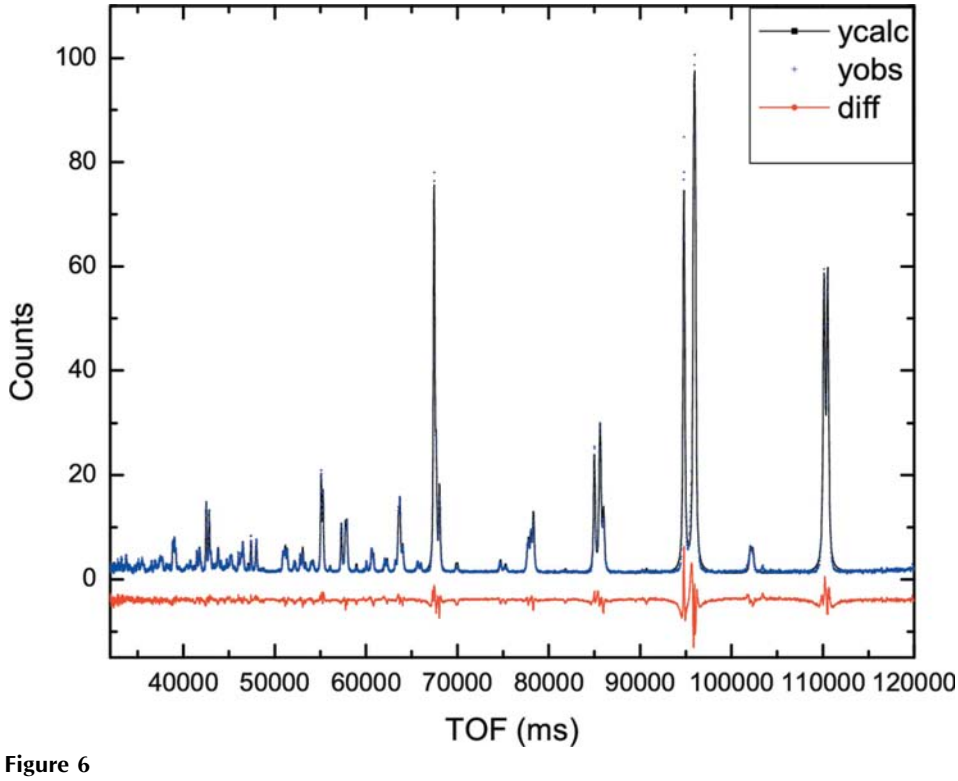

Figure 6
Room-temperature neutron time-of-flight scan from HRPD for KNN30.

3.3. Oxygen octahedra distortions in KNN30

The oxygen octahedra are significantly distorted, as demonstrated by the O—Nb—O bond angles in Table 2. Working out the tilt angles from the lattice parameters (Mitchell, 2002) gives $\theta = 5.95°$, which corresponds to a rotation about the pseudocubic [110] axis. However, the other two tilt angles, φ and Φ, which give rotations of the octahedra about the pseudo-cubic [001] and [111], respectively, could not be calculated. This method of calculation assumes that the oxygen octahedra are not distorted, whereas they certainly are (Table 2 and Fig. 8). In examining these structural distortions and tilt angles, we have not found a significant structural change in the $x = 0.3$ region, where Glazer & Ahtee found the transition from phase L to phase K. Fig. 5 shows that from our study, phase L is retained for values of x between 0.36 and 0.24. Thus, the phase boundary between K and L either does not exist or occurs below $x = 0.24$. It is therefore suggested that the physical properties and structures in the $x = 0.17$ region of the phase diagram should be investigated, where we now predict a large change in the structure from phase L to phase Q, without the intermediate step of phase K.

3.4. High-temperature phase transition of KNN30 and KNN26

The high-temperature tetragonal phase of KNN30 was refined in space group *P*4*mm* (Table 1). No oxygen octahedra tilt peaks were present, in contrast to previously published data (Ahtee & Glazer, 1976), and so the simple polar *P*4*mm* space group was adopted. A new region of phase coexistence was observed in a 10 K temperature interval from 473 to 483 K for a sample of KNN26. This pattern was indexed as a coexistence of the monoclinic and tetragonal phases, which refines well, and is consistent with the first-order nature of the phase transition. This is also indicated by the variation in lattice parameters (Fig. 9). The sample in question had well defined tilt peaks, and it was possible to see the effect of the phase transition on these peaks by X-ray diffraction. In the coexistence region, the 301 and 321 tilt peaks close to the pseudocubic 111 peak at 39.33° in 2θ decrease in intensity and move apart. They remain over a small temperature range (10–20 K) in the tetragonal phase, with their intensities steadily decreasing. This suggests that there may be an intermediate phase that has small octahedral tilts, before they disappear and the space group becomes *P*4*mm*. The narrowing of the 111 peak to a singlet in this

region suggests that the symmetry here is orthorhombic (at the lowest), if not tetragonal.

4. Conclusions

The room-temperature phase of KNN30 has been refined in monoclinic space group *Pm* and the tilt/displacement system has been shown to be $a^0_+b^+_0c^0_+$. The high-temperature polar tetragonal phase has been refined as *P*4*mm*, which is consistent with the absence of any tilt peaks. A coexistence region has been observed in a 10 K temperature interval, which appears to be a mix of the phases on either side, with evidence that there is an intermediate phase that briefly exhibits small tilting, which is either tetragonal or orthorhombic. The presence of no minus tilts below the previously reported boundary at $x = 0.3$ has implications for the physical properties in the $x = 0.17$ region, where the $a^-b^+c^-$ phase Q is expected. Such a large change in the structure over a small compositional change could potentially lead to enhanced physical properties, if indeed a phase boundary or MPB exists in that region, and this will be investigated further. Analysis around the previously reported phase boundaries at $x = 0.5$ and 0.3, which are sometimes referred to as MPBs, suggests that no first-order structural change with composition are present, and perhaps a re-definition of these phase boundaries is therefore required.

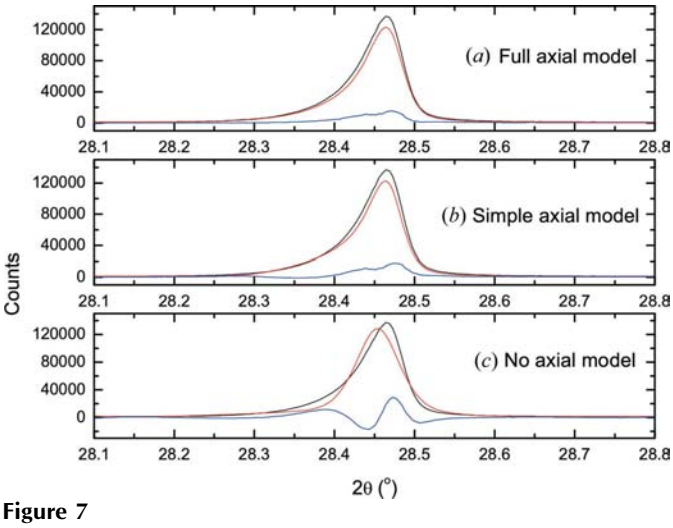

Figure 7
Comparison of (*a*) full, (*b*) simple and (*c*) no axial model for silicon 111 peak collected using the MPD with the X'celerator detector.

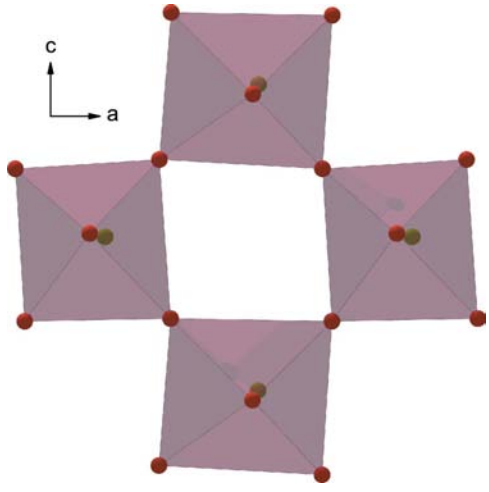

Figure 8
Diagram illustrating the distortion and tilting of the oxygen octahedra in KNN30

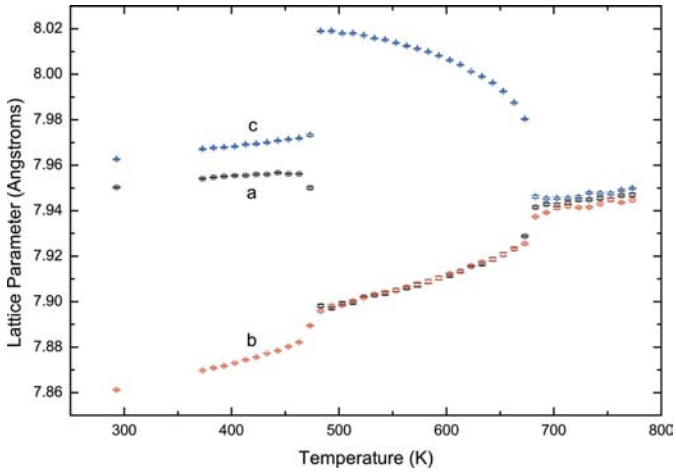

Figure 9
Lattice parameters as a function of temperature for KNN30, obtained from Rietveld refinement using neutron powder data from HRPD in *TOPAS Academic* (Coelho, 2004).

The authors wish to thank Kevin Knight for his assistance at ISIS in collecting the data. This research has been funded by an EPSRC Doctoral Training Account Studentship (Warwick) and by a Clarendon Award (Oxford). The Panalytical MPD was funded by the Advantage West Midlands Science Cities project.

References

Ahtee, M. & Glazer, A. M. (1976). *Acta Cryst.* A**32**, 434–446.
Baker, D. W. & Thomas, P. A. (2009). In preparation.
Birol, H., Damjanovic, D. & Setter, N. (2006). *J. Eur. Ceram. Soc.* **26**, 861–866.
Coelho, A. A. (2004). *TOPAS Academic*, http://members.optusnet.-com.au/~alancoelho.
Du, H., Zhou, W., Luo, F., Zhu, D., Qu, S., Li, Y. & Pei, Z. (2008). *J. Phys. D*, **41**, 1–115413/5.
Glazer, A. M. (1975). *Acta Cryst.* A**31**, 756–762.
Glazer, A. M., Thomas, P. A., Baba-Kishi, K. Z., Pang, G. K. H. & Tai, C. W. (2004). *Phys. Rev. B*, **70**, 184123–184129.
Guo, Y., Kakimoto, K. & Ohsato, H. (2004). *Mater. Lett.* **59**, 241–244.
Jaeger, R. E. & Egerton, L. (1962). *J. Am. Ceram. Soc.* **45**, 209–213.
Jaffe, B., Cook, W. R. & Jaffe, H. (1971). *Piezoelectric Ceramics*. New York: Academic Press.
Jaffe, B., Roth, R. S. & Marzullo, S. (1955). *J. Res. Natl. Bur. Stand.* **55**, 239–253.
Mitchell, R. H. (2002). *Perovskites: Modern and Ancient*, p. 22. Ontario: Almaz Press.
Noheda, B., Cox, D. E. & Shirane, G. (2000). *Phys. Rev B*, **63**, 014103.
Ragini, R. R., Mishra, S. K. & Pandey, D. (2002). *J. Appl. Phys.* **92**, 3266–3274.

Rossetti, G. A., Khachaturyan, A. G., Akcay, G. & Ni, Y. (2008). *J. Appl. Phys.* **103**, 1–114113/15.
Saito, Y., Takao, H., Tani, T., Nonoyama, T., Takatori, K., Homma, T., Nagaya, T. & Nakamura, M. (2004). *Nature*, **432**, 84–87.
Shrout, T. R. & Zhang, S. J. (2007). *J. Electroceram.* **19**, 111–124.
Stokes, H. T., Kisi, E. H., Hatch, D. M. & Howard, C. J. (2002). *Acta Cryst.* B**58**, 934–938.
Zhang, S., Xia, R., Hao, H., Liu, H. & Shrout, T. R. (2008). *Appl. Phys. Lett.* **92**, 1–152904/3.
Zhang, S., Xia, R. & Shrout, T. R. (2007). *Appl. Phys. Lett.* **91**, 1–132913/3.